CHEMISTRY
A EUROPEAN JOURNAL

DOI: 10.1002/chem.200601727

Systematic Synthesis of Lanthanide Phosphate Nanocrystals

Ziyang Huo, Chen Chen, Deren Chu, Haohang Li, and Yadong Li*[a]

Abstract: Uniform $LnPO_4 \cdot x H_2O$ (Ln = Y, La–Nd, Sm–Lu) nanocrystals that have controllable 0D (spherelike), 1D (rodlike), and 2D (polygonlike) structures have been systematically synthesized by means of a hydrothermal method by using a mixed solvent of water and ethanol. Transmission electron microscopy images and SEAD (selected area electron diffraction) patterns revealed that the products are highly crystalline and have structurally uniform shapes. IR, Raman, and electron energy loss spectroscopies gave spectra that indicated that an amount of oleic acid molecules were presented at the surface of individual nanocrystals. These nanocrystals have hydrophobic surfaces and could be easily dispersed in nonpolar solvents. Moreover, a creditable synthetic mechanism for nucleation, growth, and shape evolution has been proposed. Eu^{3+} doped products were also prepared by using the same synthetic process. The Eu^{3+} doped products exhibited an orange-red luminescence that is ascribed to an electron transition within the 4f shell. Analysis of the photoluminescent spectra revealed that the optical properties are strongly dependent on their morphologies.

Keywords: hydrothermal synthesis · lanthanides · luminescence · nanostructures · phosphates

Introduction

Uniform inorganic nanocrystals (NCs) that have a well-designed composition and crystal structure can exhibit many interesting and novel, size- and shape-dependent properties.[1] As "artificial atoms", these functional NCs, with distinct sizes and shapes, will be promising building blocks for the bottom-up approach to the construction of complex superstructures and advanced architectures.[2] Owing to their many potential applications, the systematic synthesis of colloidal NCs that have desirable properties is a key issue in nanosystems.[3,4] Dramatic efforts have been made to develop new methods for the fabrication of various high-quality inorganic NCs in different systems. Although, results such as solution-based reflux methods in organic solvents, thermolysis in organic procedures and their alternatives,[5–7] have been successful, there still remains a challenge in the discovery and exploitation of a general method and unifying principle to manipulate the sizes and shapes of those same systems.

Recently, there has been an increase in interest and research into nanostructured rare-earth compounds and rare-earth-ion-doped materials, including LnF_3, Ln_2O_3, $Ln(OH)_3$, and $LnPO_4$,[8–9] owing to their critical importance in the fields of integrated optical systems, various displays, and especially for the fluorescent labeling of cells.[10] Among these, Haase and co-workers completed an important investigation into the preparation of dispersible core-shell colloidal nanoparticles ($LaPO_4$ and $CePO_4$:Tb/$LaPO_4$) in high-temperature organic solvents.[11] These nanoparticles display multicolored emissions that have a high quantum yield and have potential applications as biosensors.[12] Based on these conventional methods, dispersible zero dimensional (0D) structured $LnPO_4$ nanoparticles can be readily obtained, however, uniform 1D (rodlike) and 2D (disklike or polygonlike) nanostructured $LnPO_4$ NCs, that have regular shapes, have rarely been prepared by using the above synthetic systems.

Herein, we report a facile hydrothermal method to fabricate various uniform $LnPO_4 \cdot x H_2O$ (Ln = Y, La–Nd, Sm–Lu) NCs in a mixed solvent of water and ethanol. By using this synthetic pathway, we can manipulate the products to gain expected morphologies that can contain rodlike (rod-), rectanglelike (rect-), and hexagonlike (hex-) shapes, in addition to the traditional 0D spherelike structures. In contrast with previous methods, which need to be carried out in nonpolar organic solvents,[5–7] a large amount of ethanol and water was introduced into our synthetic systems. Moreover, oleic acid (OA) molecules are presented at the surface of the products, which endows each NC with a hydrophobic sur-

[a] Z. Huo, C. Chen, D. Chu, H. Li, Prof. Y. Li
Department of Chemistry, Tsinghua University Beijing (P.R. China)
Fax: (+86) 10-6278-8765
E-mail: ydli@tsinghua.edu.cn

face, and results in easy separation of the final products as they spontaneously separate at the bottom of the autoclave without the need for further treatment. Based on our experiments, we have also proposed a possible synthetic mechanism for nucleation, growth, and shape evolution of the NCs. Finally, Ln^{3+} doped products, as a series of important luminescent materials, have also been readily obtained by using the same synthetic process. Eu^{3+} doped $LnPO_4{\cdot}x\,H_2O$ (Ln = Y, La, Gd, Lu) NCs that have controllable shapes and sizes have been prepared successfully. If exposed to UV light, these Eu^{3+} NCs exhibit orange-red luminescence. Examination of the photoluminescent (PL) spectra revealed that the optical properties of these NCs are strongly dependent on their shapes.

Results and Discussion

Characterization of synthesized $LnPO_4{\cdot}x\,H_2O$ (Ln = Y, La, Gd, Lu) NCs: X-ray powder diffraction (XRD) patterns of as-obtained products are shown in Figure 1A,B. Figure 1A shows the typical XRD patterns of yttrium phosphate hydrate NCs. The reflection patterns can be readily indexed to that of the pure hexagonal phase of $YPO_4{\cdot}0.8\,H_2O$, (lattice constants $a = 6.833$ and $c = 6.291$ Å, $\alpha = 90.00$ and $\gamma = 120.00°$, JCPDS 42-0082). No peaks of any other phases or impurities were detected. The XRD patterns demonstrate

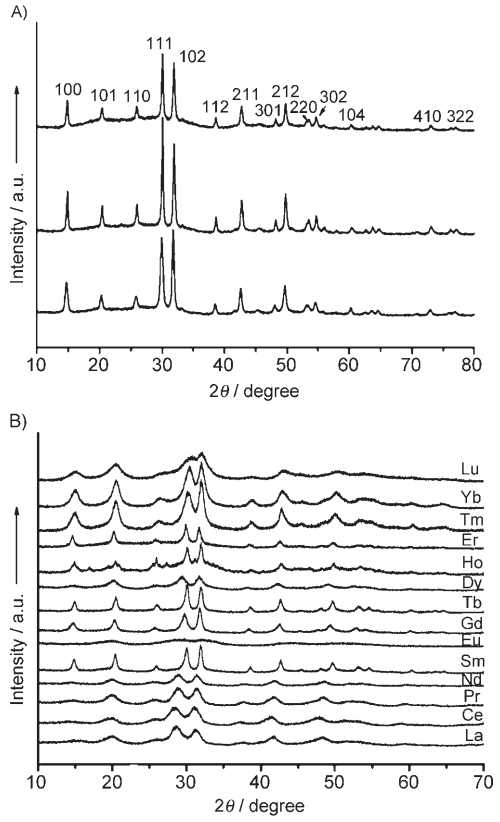

Figure 1. XRD patterns of A) rect (top), hex (middle), and rod (bottom) yttrium phosphate hydrate NCs, and B) $LnPO_4{\cdot}x\,H_2O$.

that pure-phase yttrium phosphate hydrate NCs could be obtained by our synthetic systems. The apparent broadening of some peaks is an indication of the small size of the as-obtained NCs. The Scherrer equation ($d = 0.89\lambda/B\cos\theta$) was used to calculate the size of the hex-yttrium phosphate hydrate NCs ($\approx$29 nm), which is in good agreement with the following results measured from TEM images. The other $LnPO_4{\cdot}x\,H_2O$ (Ln = La–Nd, Sm–Lu) NCs were also characterized, and their corresponding results are shown in Figure 1B.[13] These results indicate that the completely crystalline and pure-phase rare-earth phosphate hydrate products could be obtained by using hydrothermal treatment.

The size and morphology of the as-obtained NCs were examined further by high- and low-resolution transmission electron microscopy (TEM). Representative TEM images of rect-, hex-, and rod-yttrium phosphate hydrate NCs, respectively, are shown in Figure 2. A typical image of rect-NCs is shown in Figure 2A and displays the uniform structure ($\approx$25×20 nm, length × width). The selected-area electron diffraction (SAED) of rect-NCs results in the strong ring pattern from given in Figure 2B and can be well indexed to a hexagonal-phase structure. This is consistent with the XRD data given in Figure 1A. The high-resolution TEM (HRTEM) image of an individual rect-NC is shown in Figure 2C, and shows a completely crystalline structure that has lattice fringe of $\approx$3.4 Å that corresponds to the {110} lattice plane. The composition of the rect-NCs was also characterized by using energy dispersion X-ray analysis (EDXA). Analysis of the EDXA spectrum (Figure 2D) indicates that the sample is composed of Y, P, and O (the Cu signal results from the copper grid, the C signal results from the carbon membrane and the OA molecules at the surface of the NCs). The nearly monodisperse hex-NCs, that measure $\approx$15 nm in length for each side of the hexagon, can be observed clearly in Figure 2E. The HRTEM image of the hex-NCs in Figure 2F shows that the as-obtained NCs are highly crystalline and that the lattice spacing can be estimated to be $\approx$5.9 Å corresponding to the {100} lattice plane. The as-obtained NCs are rather electron sensitive, and as a consequence, after exposure to the electron beam of the HRTEM, the crystal lattices were spoiled in only a short time (several seconds). As a result, some defects appeared in the NCs, which can be observed in the HRTEM images. Notably, the as-obtained hex-NCs tended to assemble together to form high-order nanoarrays, as described previously,[14] and can be found in the TEM images presented here. The morphology of the rod-NCs can be seen in Figure 2G. Rod-NCs have an aspect ratio of $\approx$4, a diameter of $\approx$20 nm, and a length of up to $\approx$80 nm. Figure 2H shows that the rod-NCs are completely crystalline. The lattice spacing is estimated to be $\approx$2.7 Å corresponding to the {102} lattice plane.

Under the same synthetic conditions, other rare-earth phosphate hydrate NCs could also be obtained. These NCs displayed variety of uniform morphologies such as spherelike (0D), oriented rodlike (1D), and hexagonlike or disklike (2D). The typical TEM images of spherelike

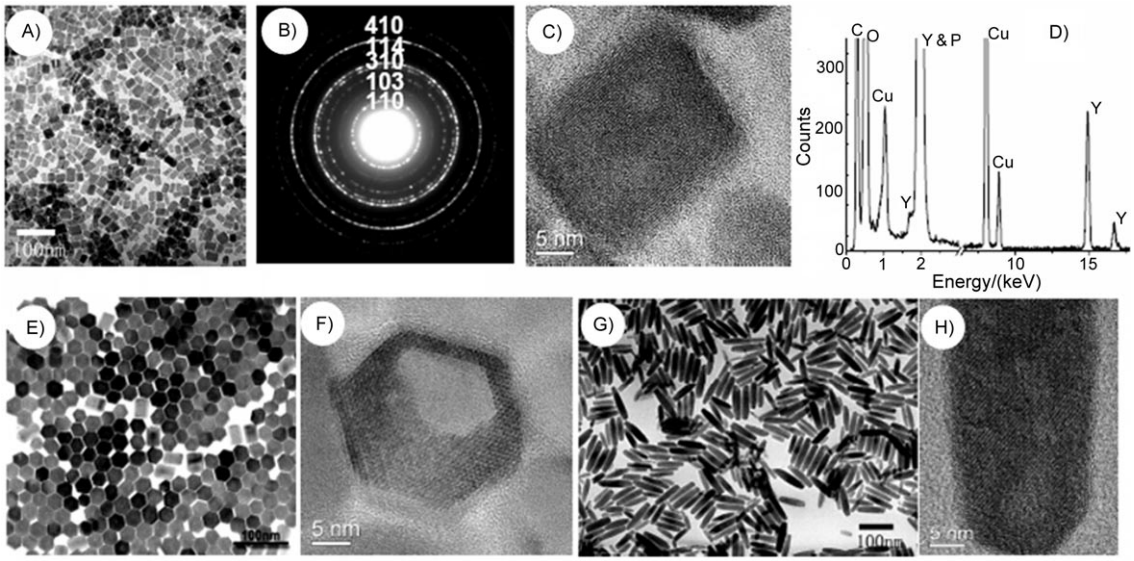

Figure 2. TEM/HRTEM images of yttrium phosphate hydrate NCs, SEAD pattern and EDXA spectrum of rect-Yttrium Phosphate hydrate NCs: A) rect-NCs, B) SEAD pattern of rect-NCs, C) HRTEM image of a rect-NC, D) EDAX spectrum of rect-NCs, E) hex-NCs, F) HRTEM image of hex-NCs, G) rod-NCs, and H) HRTEM image of rod-NCs.

$LnPO_4 \cdot x H_2O$ (Ln = La–Nd) NCs, respectively, are shown in Figure 3. The TEM image of $LaPO_4 \cdot 0.5H_2O$ NCs shown in Figure 3A displays a uniform morphology and an average

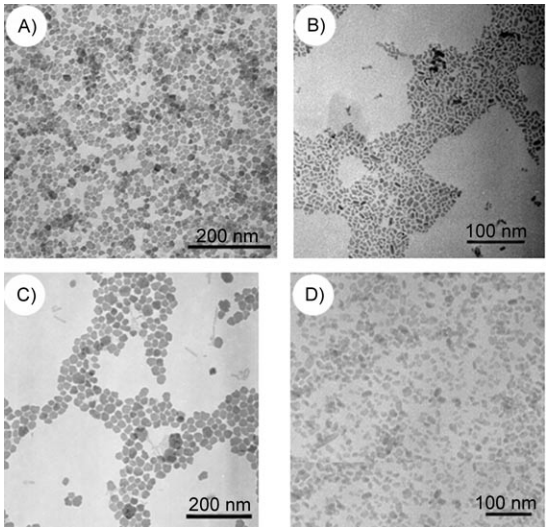

Figure 3. TEM image of $LnPO_4 \cdot x H_2O$ NCs: A) La, B) Ce, C) Pr, and D) Nd.

diameter of 13 nm. The sizes of the other $LnPO_4 \cdot x H_2O$ (Ln = Ce, Pr, Nd) NCs are 8–20 nm (Figures 3B–D) and their structural features are uniform and identical. The ionic radii of these kinds of trivalent cations (Ln^{3+}) are smaller than other lanthanide cations except for Y^{3+}. These lanthanide phosphate hydrate NCs exhibit unremarkable anisotropic properties, and irregular 0D spherelike isostructural nanoparicles are usually obtained. In Figure 4, mid-group

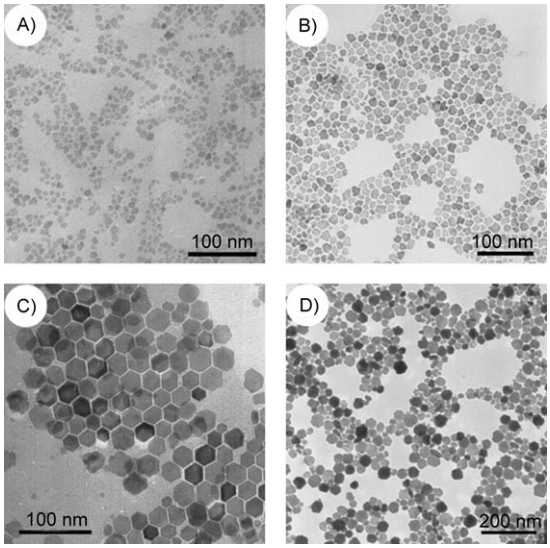

Figure 4. TEM image of $LnPO_4 \cdot x H_2O$ NCs: A) Sm, B) Eu, C) Gd, and D) Tb.

$LnPO_4 \cdot x H_2O$ (Ln = Sm–Tb) NCs are shown. Although the ionic radii are very close to those of the heavier lanthanides, various polygonlike (2D) NCs with different sizes gradually appeared. Hex-structures were found to be the most common products, which correlates to the hexagonal phase crystal structures found above. In this group, the as-obtained products seemed to show some tendency for anisotropic growth, but 1D nanostructures, such as nanorods or nanowires, were rarely observed. As shown in Figure 5, uniform hex- or rod-$LnPO_4 \cdot x H2O$ (Ln = Dy–Lu) NCs were readily synthesized by using our system. In this group, all of the as-obtained NCs have regular shapes with different sizes. The

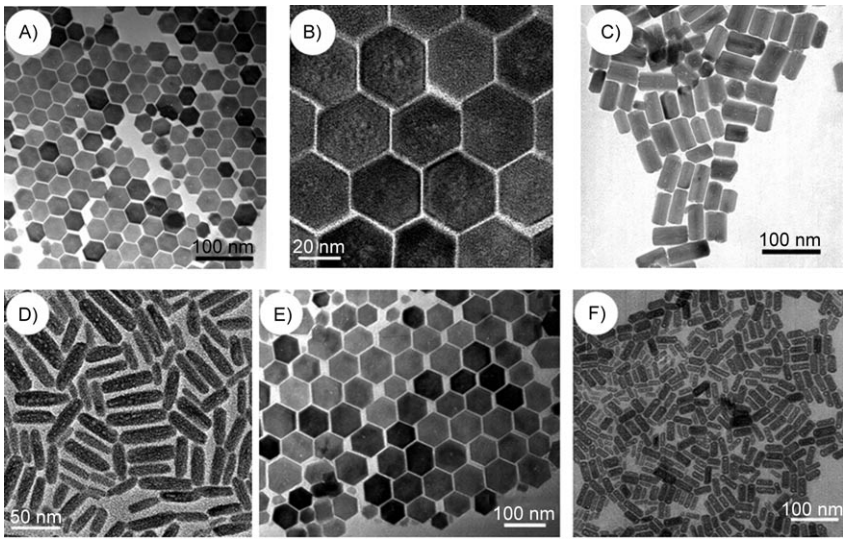

Figure 5. TEM image of $LnPO_4 \cdot x H_2O$ NCs: A) Dy, B) Er, C) Ho, D) Tm, E) Yb, and F) Lu.

size distribution can be addressed by dynamic light scattering (DLS), which was used to elucidate $DyPO_4$ and $YbPO_4$ NCs, respectively, in Figure 6. The distribution of the diameters of $DyPO_4$ NCs fall in the 40–60 nm range, and the peak is at 46.8 nm (Figure 6A). The distribution of $YbPO_4$ NCs falls around 90 nm (Figure 6B). These results indicate that the particle size distributions of these NCs are partially broad. In contrast with the above two groups, some 1D nanostructures that have different aspect ratios were also synthesized; therefore, the more evident tendency of anisotropic growth can be addressed. The heavy lanthanide NCs in this group have larger ionic radii than the other lighter lanthanides. However, although Y^{3+} is much lighter in weight than the heavy lanthanides, the morphologies and sizes of the as-obtained yttrium phosphate hydrate NCs are much closer to these heavy lanthanide phosphates. This finding is supported by the lattice parameter of Y^{3+}, which is also close to these heavy lanthanide cations. Therefore the various yttrium phosphate hydrate NCs produced should also fall into the heavier lanthanide NC group.

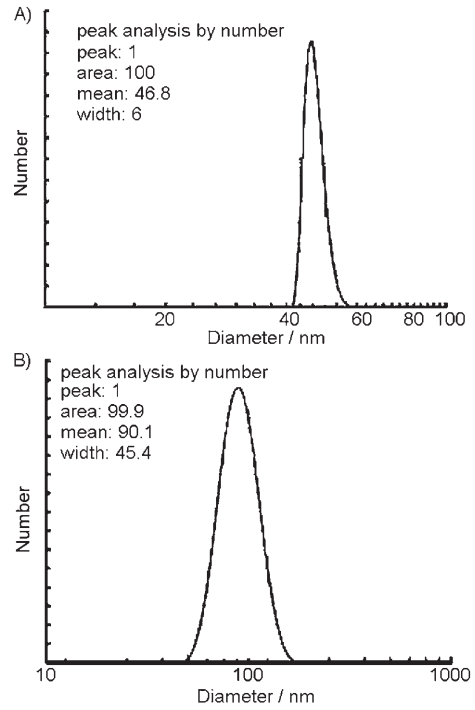

Figure 6. Size distributions of A) $DyPO_4$, and B) $YbPO_4$ analyzed by DLS

In our systems, all the NCs disperse well in nonpolar solvents, such as hexane, chloroform, and toluene, to form transparent colloid solutions. Upon addition of alcohol to the above solutions, the NCs spontaneously aggregate, and consequently, precipitate at the bottom of the vessel. The precipitation was collected and the upper superfluous solvent removed, the NCs can be re-dispersed in nonpolar solvents. This convenient redispersity comes from the hydrophobic surfaces of the NCs, which were formed by OA molecules that are presented at the surface of the products. Evidence for this can be produced by using FT-IR, Raman, and electron energy loss spectroscopies. The related spectra can be found in Figure 7, in which all of the characteristic spectra has been taken from rect-$YPO_4 \cdot 0.8 H_2O$ NCs. The FT-IR spectrum, as shown in Figure 7A, displays peaks at $\tilde{\nu} = 542$ and 623 cm^{-1}, and a broad band centered between 1078 and 1012 cm^{-1}, these peaks represent the hexagonal $YPO_4 \cdot 0.8 H_2O$. The band in the region $\tilde{\nu} = 1675$–$1760\ cm^{-1}$ is attributed to the $\tilde{\nu}$(C=O) stretch, and the band at 1630 cm^{-1} is attributed to C=C vibrations. The broad bands from $\tilde{\nu} = 1506$–$1573\ cm^{-1}$ are assigned to the antisymmetric $\tilde{\nu}$(COO−) and the symmetric $\tilde{\nu}$-(COO−) stretches. The peaks at $\tilde{\nu} = 2850$ and 2922 cm^{-1} are attributed to the symmetric and antisymmetric methylene stretches.[15] The broad vibration band centered at $\tilde{\nu} = 3510\ cm^{-1}$ is assigned to the O−H stretch. These specific results demonstrate the existence of oleic acid molecules, and moreover, the Raman spectrum (Figure 7B) also supports these conclusions. The two bands centered at 1663 and 1440 cm^{-1} are attributed to C=O and COO− vibrations, respectively. The peak at 1260 cm^{-1} and the broad band from 2800 cm^{-1} to 3000 cm^{-1} are ascribed to alkyl chain vibrations. Electron energy loss spectroscopy (EELS) by core-level excitations, taken from the edge of the NCs, is shown in Figure 7C: The observed initial peak in the carbon K-edge spectrum located around 285 eV is attributed to $1s \rightarrow \pi^*$ transitions, which indicates that the carbon atoms in the products are sp^2 hybridized, this is in agreement with the ex-

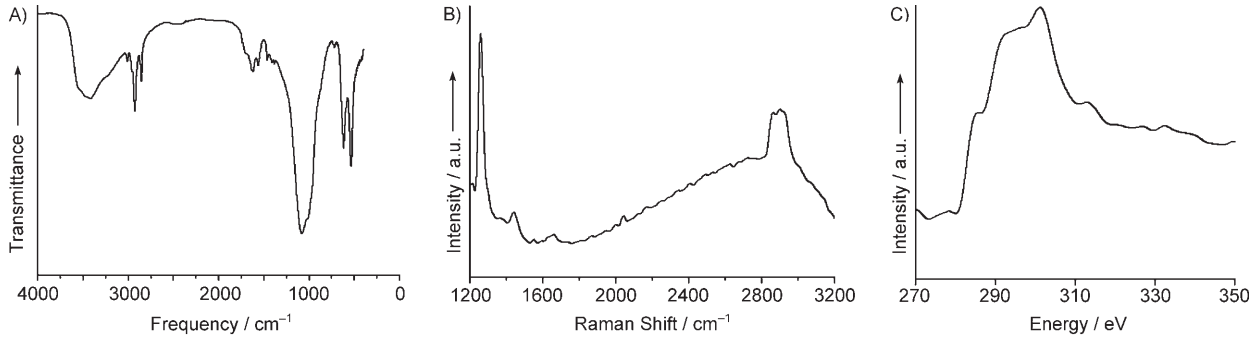

Figure 7. The A) FTIR spectrum, B) Raman spectrum, and C) EELS of rect-$YPO_4{\cdot}0.8\,H_2O$ NCs.

istence of C=C bonds that belong to OA molecules. The energy loss starting at 291 eV is ascribed to the $1s \rightarrow \sigma^*$ transitions of the carbon atoms. Summing up the characterized results here, it would be easy to deduce that an amount of OA molecules are present at the surface of the NCs. The OA molecules present endow the NCs with a hydrophobic surface and, consequently, the NCs disperse well in nonpolar solvents. The OA molecules absorbed on the surface of the NCs, through the noncovalent interactions generated from the overlap of the long chain alkyl, enable the self-assembly of nano-building blocks for use in the construction of high-order superstructures and controllable architectures.[14,16]

Proposed controlled synthesis and formation mechanism: To prepare different $LnPO_4{\cdot}x\,H_2O$ NCs, the kinetics of their growth has to be monitored and manipulated. The proposed synthetic process and mechanism for the synthesis of NCs is described in Figure 8. The aqueous solution containing Ln^{3+}

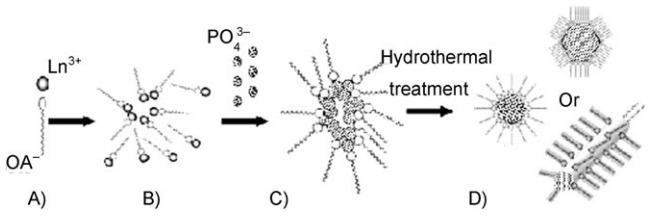

Figure 8. Schematic illustration of our proposed synthetic and formation mechanism

was added to the water-ethanol solvent. In this case the Ln^{3+} ions are hard and acidic, their polarization and distortion are quite uncommon, and they have a moderate affinity for oxygen. Moreover, owing to the existence of a large amount of sodium oleate (NaOA), a result of mixing NaOH and OA in the above solvent, Ln^{3+} was capped by OA through a reversible ion exchange process,[9b,17] as shown in Figure 8A,B (for clarity, the OA molecules were magnified individually). Subsequently, an aqueous solution containing PO_4^{3-} was added to react with the Ln^{3+}, and as a consequence, the basic complex monomers were fabricated. Some of these basic monomers aggregated together. At the same time, both homogeneous and amorphous precipitates were formed (Figure 8C). Hydrothermal methods have been shown to be an effective synthetic means to preparing various nanostructures,[8b,9] so the above as-obtained amorphous precipitates were transferred to an autoclave and subjected to hydrothermal treatment at specific temperatures. Because a large amount of OA molecules exist as capping agents in the system, the crystalline nuclei formed slowly in the early stages, after which, the NCs grew uniformly and gradually. Finally, the growth of the as-obtained NCs was terminated by the in-situ generated OA molecules absorbed at the surface (Figure 8D). Owing to the polar environment adopted by this synthesis, the products spontaneously separated in the bottom of autoclave.

It should be noted that yttrium phosphate hydrate NCs with various uniform shapes and sizes could be obtained in our systems. A result, which is clearly related to the concentration of OA and NaOH, as well as the $[PO_4^{3-}]/[Ln^{3+}]$ ratio. If the $[PO_4^{3-}]/[Ln^{3+}]$ ratio is fixed at 1:1, an increase in the concentration of OA and NaOH (a double dose was adopted to obtain hex-NCs) led to a shape evolution of the products from the rect-structure to the hex-structure (Figure 2A,E). The concentration of OA and NaOH was fixed at a high level, and an increase in the $[PO_4^{3-}]/[Ln^{3+}]$ ratio-induced growth of 1D NCs that had different sizes, as shown in Figure 2G ($[PO_4^{3-}]/[Ln^{3+}]=1.5$) and Figure 9 ($[PO_4^{3-}]/[Ln^{3+}]=2$ and $[PO_4^{3-}]/[Ln^{3+}]=2.5$). As the ratio of $[PO_4^{3-}]/[Ln^{3+}]$ increases, the size of these rod-NCs increases dramatically. The larger rod-NCs shown in Figure 9 cannot be dispersed in apolar solvent as the others. From these results, it can be evidenced that the $[PO_4^{3-}]/[Ln^{3+}]$ ratio is an important factor in guiding the anisotropic growth. Increas-

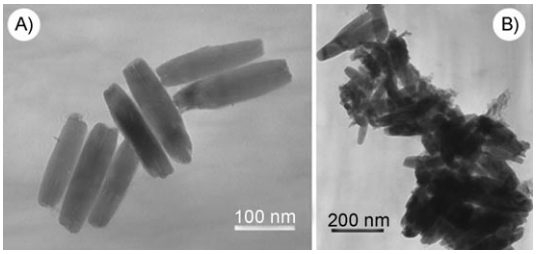

Figure 9. TEM image of $YPO_4{\cdot}0.8\,H_2O$ NCs obtained by using different ratios of $[PO_4^{3-}]/[Ln^{3+}]$: A) $[PO_4^{3-}]/[Ln^{3+}]=2$, B) $[PO_4^{3-}]/[Ln^{3+}]=2.5$

ing the concentration of PO_4^{3-} accelerated the rate of reaction and shifted the reaction equilibrium towards the positive direction, leading to the presence of a higher monomer concentration. In this regard, the clear anisotropic tendency displayed here agrees with Gibbs-Thompson theory and previous concept, that a higher monomer concentration will encourage 1D nanostructural growth.[11,18]

Optical properties of Eu^{3+} doped $LnPO_4 \cdot x H_2O$ (Ln = Y, La, Gd, and Lu) NCs: The luminescence of rare-earth ions originates from electron transitions within the 4f shell. Here, the 4f shells of Y^{3+}, La^{3+}, and Lu^{3+} are either empty or completely filled, so no f→f transitions are possible. Furthermore, the 4f shell of Gd^{3+} (election configuration: $4d^{10}4f^7$) is half-filled, so no f→f transitions can break this stable configuration. Hence the phosphates of these Ln^{3+} (Ln = Y^{3+}, La^{3+}, $Gd^{3+}$and Lu^{3+}) are transparent in the visible spectra region and can serve as desirable host materials for other Ln^{3+} ions.[9,11] In this work, the optical properties of Eu^{3+} doped $LnPO_4 \cdot x H_2O$ (Ln = Y^{3+}, La^{3+}, Gd^{3+}, and Lu^{3+}) NCs were investigated, and all the Eu^{3+} doped products were prepared by the same synthetic pathway without the high-temperature annealing. This doping process alters neither the crystal structures nor the shapes of the host materials. Room-temperature emission spectra are presented in Figure 10. The Eu^{3+} doped samples primarily exhibit orange-red luminescence (λ = 570 to 700 nm) of different intensities, which correspond to transitions from the excited $^5D_0$ levels to the ^7F_J (J = 0–4). In Figure 10A, it should be noted that the intensities of $^5D_0 \rightarrow {}^7F_1$ transition, and $^5D_0 \rightarrow {}^7F_2$ transition, are quite different between various $YPO_4 \cdot 0.8 H_2O$/Eu NCs. The emission spectrum of Eu^{3+} is very sensitive to the local environment. The $^5D_0 \rightarrow {}^7F_1$ transition is a magnetic dipole transition, which is greatly affected by the local symmetry.[9,14,19,20] Namely, if more Eu^{3+} is present in the inversion sites, the emission intensity from the $^5D_0 \rightarrow {}^7F_1$ transition will be enhanced and the product will primarily exhibit orange luminescence.[20,21] The inverse is also true, if less Eu^{3+} is present, the more $^5D_0 \rightarrow {}^7F_2$ transitions (electronic transition) will occur. For hex-structures, there are more atoms at the surface of the NCs, owing to the shape effect, which leads to a lower coordination number and less chance that Eu^{3+} ions will appear in the inversion site. Hence, the hex-$YPO_4 \cdot 0.8 H_2O$:Eu NCs mainly exhibit a red luminescence. On the other hand, rod-NCs have fewer surface atoms and more Eu^{3+} ions in the inversion sites, so this situation would enhance the $^5D_0 \rightarrow {}^7F_1$ transition. It is clear that the optical properties of Eu^{3+} doped samples depend greatly on the morphologies of the host materials.

Conclusion

In summary, a general synthetic pathway for preparation of various $LnPO_4 \cdot 0.8 H_2O$ NCs that have uniform controllable shapes, including 1D and 2D structures, has been described.

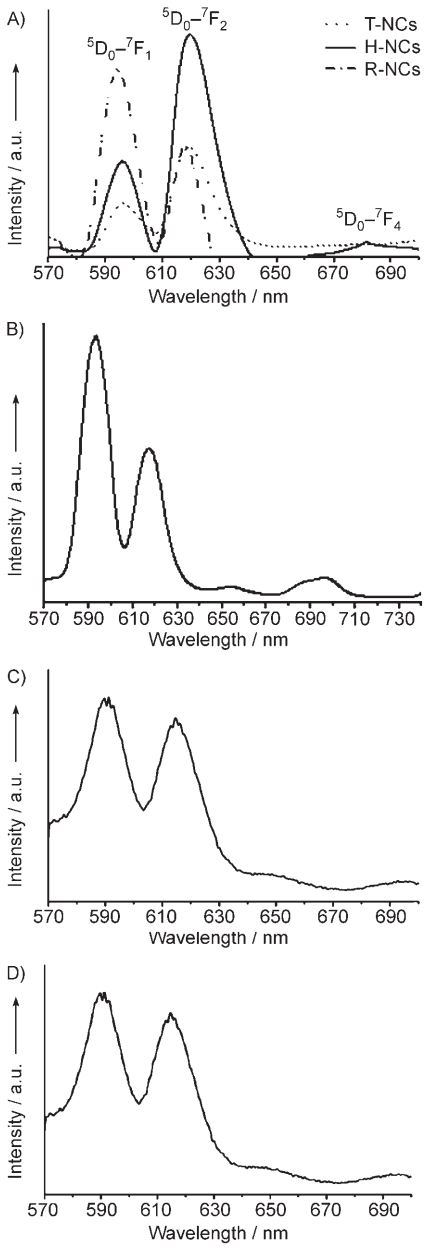

Figure 10. The photoluminescent spectra of $LnPO_4 \cdot x H_2O$ LnPO4:Eu-(10%) NCs (λ_{exc} = 258 nm): A) rect-/hex-/rod-$YPO_4 \cdot 0.8 H_2O$, B) $LaPO_4 \cdot 0.5 H_2O$, C) $GdPO_4 \cdot H_2O$ NCs, and D) $LuPO_4 \cdot 0.5 H_2O$ NCs.

A series of characterization has proved that oleic acid (OA) molecules are present at the surface of the lanthanide phosphate nanocrystals. These products have hydrophobic surfaces and could be easily re/dispersed in nonpolar solvent. Systematic investigation of the formation of NCs has led to a considered and reasonable synthetic mechanism. The way that the concentration of OA and NaOH, as well as the $[PO_4^{3-}]/[Ln^{3+}]$ ratio, plays a very important role in governing the dynamic process has also been discussed. Owing to f→f transitions, Eu^{3+}-doped NCs exhibit orange-red luminescence after excitation by ultraviolet light. The photoluminescent spectra of Eu^{3+}-doped NCs, show that the optical prop-

erties are significantly affected by the morphologies of the NCs. It is believed that this work will help us to comprehend how kinetic factors govern growth tendencies, and moreover, the proposed synthetic pathway may open an avenue to enable us to tailor the structures, composition, and morphologies of various nano-objects for consequent use in related fields.

Experimental Section

All chemicals were of analytical grade, and were used as received without further treatment. Deionized water was used throughout. In a typical synthesis, NaOH (0.6 g) was added to a solution of oleic acid (10 mL) in ethanol (10 mL). This mixture was stirred. A solution of NaH_2PO_4 (5 mL, 0.2 mmol L^{-1}) and a aqueous solution of $Ln(NO_3)_3$ (5 mL, 0.2 mmol L^{-1}) were added to the reaction mixture. Some precipitates of amorphous $LnPO_4$ appeared immediately. After stirring for a while, the mixture was transferred into an autoclave (50 mL), and then, additional ethanol (15 mL) was added. The autoclave was sealed and then the contents was heated to 140 °C for 8 h. The system was then allowed to cool to room temperature. The final products spontaneously separated in the bottom of the autoclave. Eu^{3+} doped samples were prepared as above, except that 10 % (total molar ratio) $Eu(NO_3)_3$ was added. The products were characterized by using an X-ray diffractometer (Rigaku D/max 2500Pc, $Cu_{k\alpha}$ radiation, $\lambda = 1.5418$ Å). The operation voltage and current were kept at 40 KV and 250 mA, respectively. The sizes and morphologies of the NCs were examined by using a transmission electron microscope (JEOL JEM-1200EX) and a high-resolution transmission electron microscope (Tecnai F20). SAED patterns were recorded by transmission electron microscopy. Raman (Renishaw RM 1000, excitation wavelength 514 nm) and Fourier transform infrared spectra (Perkin-Elmer Spectrometer GX) were used to characterize the structure of the samples. Electron energy loss spectra measurements were performed by using a Gantan parallel detection spectrometer attached to a transmission electron microscope (JEOL JEM-2010F). Fluorescent spectra were recorded by using a Fluorescence Spectrophotometer (Hitachi F-4500). Dynamic light scattering was performed by using a Malvern Zetasizer 3000 HS.

Acknowledgements

This work was supported by NSFC (90406003 and 90606006), a Foundation grant for Authors of Nationally Excellent Doctoral Dissertations by the P.R. China, and the State Key Project of Fundamental Research for Nanomaterials and Nanostructures (2006CBON0300).

[1] a) A. P. Alivisatos, *Science* **1996**, *271*, 933–937; b) C. B. Murray, C. R. Kagan, M. G. Bawendi, *Annu. Rev. Mater. Sci.* **2000**, *30*, 545–610.
[2] a) C. B. Murray, C. R. Kagan, M. G. Bawendi, *Science* **1995**, *270*,1335–1338; b) C. T. Black, C. B. Murray, R. L. Sandstrom, S. H. Sun, *Science* **2000**, *290*, 1131–1134; c) M. P. Pileni, *Langmuir* **1997**, *13*, 3266–3276.
[3] W. W. Yu, X. G. Peng, *Angew. Chem.* **2002**, *114*, 2474–2477; *Angew. Chem. Int. Ed.* **2002**, *41*, 2368–2371, and reference therein.
[4] X. Wang, J. Zhuang, Q. Peng, Y. D. Li, *Nature* **2005**, *437*, 121–124.
[5] S. H. Sun, C. B. Murray, *J. Appl. Phys.* **1999**, *85*, 4325–4330.
[6] J. Park, K. J. An, Y. S. Hwang, J. G. Park, H. J. Noh, J. Y. Kim, J. H. Park, N. M. Hwang, T. Hyeon, *Nat. Mater.* **2004**, *3*, 891–895.
[7] L. Manna, D. J. Milliron, A. Meisel, E. C. Scher, A. P. Alivisatos, *Nat. Mater.* **2003**, *2*, 382–385.
[8] a) J. C. Boyer, F. Vetrone, L. A. Cuccia, J. A. Capobianco, *J. Am. Chem. Soc.* **2006**, *128*, 7444–7445; b) H. Pedersen, L. Ojamae, *Nano Lett.* **2006**, *6*, 2004–2008.
[9] a) Y. P. Fang, A. W. Xu, R. Q. Song, H. X. Zhang, L. P. You , J. C. Yu, H. Q. Liu, *J. Am. Chem. Soc.* **2003**, *125*, 16025–16034; b) R. X. Yan, X. M. Sun, X. Wang, Q. Peng, Y. D. Li, *Chem. Eur. J.* **2005**, *11*, 2183–2195.
[10] a) L. Y. Wang, R. X Yan, Z. Y. Huo, L. Wang, J. H Zeng, J. Bao, X. Wang, Q. Peng, Y. D. Li, *Angew. Chem.* **2005**, *117*, 6208–6211; *Angew. Chem. Int. Ed.* **2005**, *44*, 6054–6057; b) G. S Yi, H. C. Lu, S. Y Zhao, Y. Ge, W. J. Yang, D. P. Chen, L. H Guo, *Nano Lett.* **2004**, *4*, 2191–2196; c) L. Y. Wang, Y. D. Li, *Chem. Commun.* **2006**, 2557–2559.
[11] a) H. Meyssamy, K. Riwotzki, A. Kornowski, S. Naused, M. Haase, *Adv. Mater.* **1999**, *11*, 840–844; b) K. Riwotzki, H. Meyssamy, A. Kornowski, M. Haase, *J. Phys. Chem. B* **2000**, *104*, 2824–2828; c) O. Lehmann, K. Kömpe, M. Haase *J. Am. Chem. Soc*, **2004**, *126*, 14935–14942.
[12] F. Meiser, C. Cortez, F. Caruso, *Angew. Chem.* **2004**, *116*, 6080–6083; *Angew. Chem. Int. Ed.* **2004**, *43*, 5954–5957.
[13] $LaPO_4{\cdot}0.5H_2O$ (JCPDS 46-1439), $CePO_4{\cdot}H_2O$ (JCPDS 35-0614), $PrPO_4{\cdot}H_2O$ (JCPDS 46-1439), $NdPO_4{\cdot}0.5H_2O$ (JCPDS 34-0505), $SmPO_4{\cdot}0.5H_2O$ (JCPDS 34-0537), $EuPO_4{\cdot}H_2O$ (JCPDS 20-1044), $GdPO_4{\cdot}H_2O$ (JCPDS 39-0232), $TbPO_4{\cdot}H_2O$ (JCPDS 20-1244), $DyPO_4{\cdot}1.5H_2O$ (JCPDS 20-0385), $HoPO_4{\cdot}2H_2O$ (JCPDS 20-0475), $ErPO_4{\cdot}0.9H_2O$ (JCPDS 42-0083), $TmPO_4{\cdot}3H_2O$ (JCPDS 20-1289), $YbPO_4{\cdot}0.4H_2O$ (JCPDS 54-1044), $LuPO_4{\cdot}0.5H_2O$ (JCPDS 54-1015).
[14] Z. Y. Huo, C. Chen, Y. D Li, *Chem. Commun.* **2006**, 3522–3524.
[15] F. Soderlind, H. Pedersen, R. M. Petoral, P. O. Kall, K. Uvdal, *J. Colloid Interface Sci.* **2005**, *288*, 140–148.
[16] a) M. Li, H. Schnablegger, S. Mann, *Nature* **1999**, *402*, 393–395; b) M. M. Maye, I. S. Lim, J. Luo, Z. Rab, D. Rabinovich, T. B. Liu, C. J. Zhong, *J. Am. Chem. Soc.* **2005**, *127*, 1519–1529.
[17] a) X. G. Peng, *Adv. Mater.* **2003**, *15*, 459–463; b) K. Riwotzki, H. Meyssamy, H. Schnablegger, A. Kornowski, M. Haase, *Angew. Chem.* **2001**, *113*, 574–578; *Angew. Chem. Int. Ed.* **2001**, *40*, 573–576; c) A. L. Rogach, D. V. Talapin, E. V. Shevchenko, A. Kornowski, M. Haase, H. Weller, *Adv. Funct. Mater.* **2002**, *12*, 653–664; d) M. Chen, J. P. Liu, S. Sun, *J. Am. Chem. Soc.* **2004**, *126*, 8394–8395.
[18] Z. A. Peng, X. G. Peng, *J. Am. Chem. Soc.* **2001**, *123*, 183–184.
[19] R. X. Yan, Y. D. Li, *Adv. Funct. Mater.* **2005**, *15*, 763–770.
[20] B. R. Judd, *Phys. Rev.* **1962**, *127*, 750.
[21] a) E. T. Goldburt, B. Kulkarni, R. N Bhargava , J. Taylor , M. Libera, *J. Lumin.* **1997**, *72–4*, 190–192; b) D. Zakaria, R. Mahiou, D. Avignant, M. Zahir, *J. Alloys Compd.* **1997**, *257*, 65–68.

Received: December 4, 2006
Published online: June 21, 2007

